Surv Geophys (2016) 37:27–45
DOI 10.1007/s10712-015-9351-1

Earth's Electromagnetic Environment

Catherine Constable[1]

Received: 28 April 2015 / Accepted: 17 November 2015 / Published online: 1 December 2015

Abstract The natural spectrum of electromagnetic variations surrounding Earth extends across an enormous frequency range and is controlled by diverse physical processes. Electromagnetic (EM) induction studies make use of external field variations with frequencies ranging from the solar cycle which has been used for geomagnetic depth sounding through the 10^{-4}–10^{4} Hz frequency band widely used for magnetotelluric and audio-magnetotelluric studies. Above 10^{4} Hz, the EM spectrum is dominated by man-made signals. This review emphasizes electromagnetic sources at $\sim$1 Hz and higher, describing major differences in physical origin and structure of short- and long-period signals. The essential role of Earth's internal magnetic field in defining the magnetosphere through its interactions with the solar wind and interplanetary magnetic field is briefly outlined. At its lower boundary, the magnetosphere is engaged in two-way interactions with the underlying ionosphere and neutral atmosphere. Extremely low-frequency (3 Hz–3 kHz) electromagnetic signals are generated in the form of sferics, lightning, and whistlers which can extend to frequencies as high as the VLF range (3–30 kHz).The roughly spherical dielectric cavity bounded by the ground and the ionosphere produces the Schumann resonance at around 8 Hz and its harmonics. A transverse resonance also occurs at 1.7–2.0 kHz arising from reflection off the variable height lower boundary of the ionosphere and exhibiting line splitting due to three-dimensional structure. Ground and satellite observations are discussed in the light of their contributions to understanding the global electric circuit and for EM induction studies.

Keywords Electromagnetism · Geomagnetic spectrum · Ionosphere · Schumann resonance · Sferics · Lightning · Magnetotellurics · Audio-magnetotellurics

✉ Catherine Constable
cconstable@ucsd.edu

[1] Institute of Geophysics and Planetary Physics, Scripps Institution of Oceanography, University of California at San Diego, La Jolla, CA 92093-0225, USA

1 Introduction

Earth's magnetic environment is shaped by its dominantly dipolar internal magnetic field and its dynamic interaction with the fully ionized plasma that constitutes the solar wind. The pressure balance between them defines the magnetopause, the boundary of the region called the magnetosphere that is dominated by the geomagnetic field. The ionosphere is a partially ionized gas sandwiched between the neutral density atmosphere and the larger magnetosphere. Enhanced currents flow in the dayside ionosphere as a result of the diurnal cycle of solar heating. Below the ionosphere, lightning activity (sferics) in the neutral atmosphere is responsible for much of the electromagnetic activity at frequencies above 1 Hz. Kinetic energy and electromagnetic energy are provided to the magnetosphere, ionosphere, and upper atmosphere by the solar wind depositing charged particles into Earth's magnetosphere, largely via the polar regions. The solar wind controls space weather and climate, and retention of Earth's atmosphere is generally attributed to the internal magnetic field preventing widespread stripping of volatiles by the solar wind.

This review will emphasize electromagnetic sources at ~ 1 Hz and higher, which includes parts of the ultralow frequency (ULF) range $f < 3$ Hz, the extremely low frequency (ELF) band, $3 < f < 3 \times 10^3$ Hz, and the VLF range from 3 to 30 kHz. These sources provide information about the upper atmosphere (ionosphere and magnetosphere) as well as the lower atmosphere and electrical structure of Earth's lithosphere. It is important to understand their place in the geomagnetic spectrum and that knowledge of ionospheric processes is informed by developments in both magnetospheric and atmospheric science. In Sect. 2, the main focus will be on the frequency spectrum of variations, the internal magnetic field, and its separation from the high-frequency external variations. This will be followed in Sects. 3 and 4 by brief descriptions of the structure of the magnetosphere, the ionosphere, and their interactions with the upper atmosphere, before we turn to discussion of the global electric circuit (Sect. 5), and the role of sferics in the origin and structure of ELF fields and the Schumann resonance.

Finally, in Sect. 6, we return to some major applications of EM signals at frequencies >1 Hz. Whistlers and related ionospheric phenomena in the VLF range (Helliwell 2006) were first identified in the late nineteenth century and early twentieth century, and subsequent research alerted the community to the importance of these signals in the study of the outer ionosphere and magnetosphere, satellite communications, nuclear detection, and general solar terrestrial relationships. During the cold war, considerable interest was generated in the idea of using the ionospheric waveguide for global communications with submarines. More recently, there has been a surge in activity related to understanding the global atmospheric electrical circuit and especially changes in thunderstorm and lightning activity in studies of global warming and climate variations. The source field provided by the propagation of EM signals from sferics as waves through the insulating atmosphere finds widespread use in audio-magnetotelluric (AMT) near-surface sounding in both industrial and academic settings. The small fraction of the signal transmitted into the ground induces electrical currents that diffuse into Earth with a skin depth dependent on both frequency of the wave and subsurface conductivity. Orthogonal electric and magnetic field components are related through a frequency-dependent impedance tensor (Vozoff 1991; Simpson and Bahr 2005; Weidelt and Chave 2012) which can be inverted to recover subsurface geoelectrical structure (Constable et al. 1987; Rodi and Mackie 2001; Siripunvaraporn 2012; Rodi and Mackie 2012). The subsurface conductivity structure completes the global electric circuit (GEC), so that in addition to being important in their

own right near-surface global induction studies can be expected to play an increasingly important role in understanding Earth's electric field.

Numerous research careers have been devoted to geomagnetism and aeronomy, and I cannot hope to do justice to all in this brief review. Excellent monographs have been written on various aspects of the material to be discussed, and I urge readers to consult them where appropriate. A small selection is given here, with the goal of providing direction to better coverage of several major topics mentioned later. From a historical perspective, the two-volume work of Chapman and Bartels (1940) provides a comprehensive view of geomagnetic phenomena, supplemented by Matsushita and Campbell (1967) for the external field, and in a somewhat more current view by the four edited volumes titled *Geomagnetism* (Jacobs 1987) . The mathematical and physical foundations for describing geomagnetic phenomena are given in some detail by Backus et al. (1996). More recent coverage for internal field observations and their interpretations including some description of EM induction studies (Constable 2007) is provided in the *Treatise of Geophysics*, Vol 5, (Kono 2007), *Encyclopedia of Geomagnetism & Paleomagnetism* (Gubbins and Herrero-Bervera 2007), and *Terrestrial Magnetism* (Hulot et al. 2010). A monograph by Simpson and Bahr (2005) gives information about the practicalities of MT sounding, but is largely superseded by the comprehensive edited volume of chapters in the *The Magnetotelluric Method* (Chave and Jones 2012), detailing multiple topics ranging across basic MT theory and practice. The advent of satellite observations in the middle of the twentieth century provided a truly global perspective for observations, and this has been combined with the integration of a theoretical framework based on plasma physics and fluid dynamics. A general introduction to Earth's external EM environment is given in *Introduction to Space Physics* (Kivelson and Russell 1995) while for specifics of ionospheric studies, see for example *The Earth's Ionosphere* (Kelley 2009). Two monographs (Nickolaenko and Hayakawa 2002, 2014) are devoted to resonant EM fields produced by lightning in the Earth-ionosphere cavity. The latter contains a comprehensive review of efforts to use the Schumann resonances for global sensing of thunderstorm activity and of the lower ionosphere at a planetary scale, and a further volume (Surkov and Hayakawa 2014) is devoted to ULF and ELF EM fields. The monograph *Whistlers and Related Ionospheric Phneonemena* (Helliwell 2006) relates the history of discovery and subsequent development of studies in that area.

2 The Grand Spectrum of Magnetic Field Variations

The natural spectrum of electromagnetic variations surrounding the Earth extends across an enormous frequency range and is controlled by a variety of internal and external physical processes. Recent reviews (Sabaka et al. 2010; Olsen et al. 2010) outline the mathematical and physical bases for geomagnetic field modeling and the modern data from geomagnetic observatories, repeat stations, and low- Earth-orbiting satellites that are used to infer the structure. The separation of sources is based on spatial and temporal structures. As indicated in Fig. 1, the spatial origin of the sources can be roughly divided according to the characteristic timescales of their variations, with some (not insignificant) overlaps. Lithospheric contributions to the field are essentially static and make no contribution to the frequency spectrum, but separating them from the large-scale magnetospheric and ionospheric field variations can be troublesome because of temporal–spatial aliasing in the satellite observations that provide the best global coverage.

The overall shape of the spectrum is red, reflecting the timescale of variations in the predominantly dipolar internal field produced by the geodynamo in Earth's liquid outer core

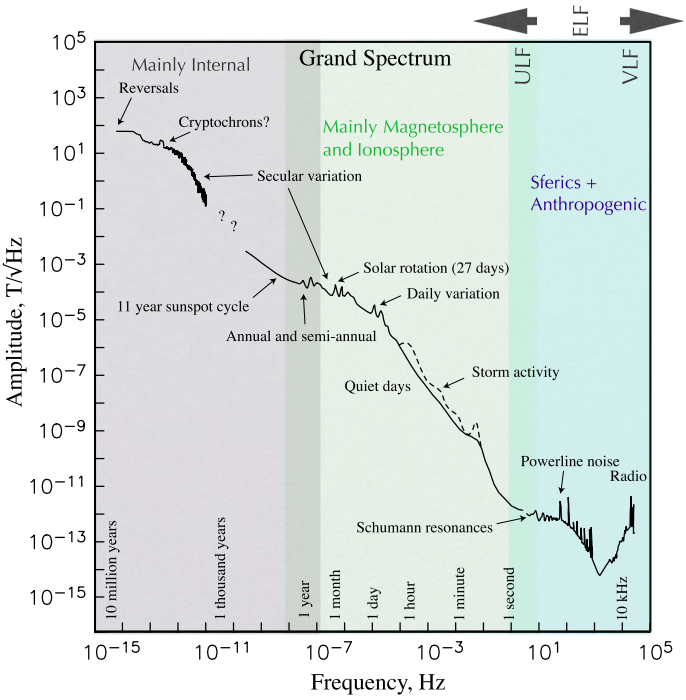

Fig. 1 Amplitude spectrum of geomagnetic variations, modified from Constable and Constable (2004)

as shown in Fig. 2. Fluid flow in the highly electrically conductive (1.1×10^6 S/m, Pozzo et al. 2012) core produces a secular variation in the magnetic field, which propagates upward through the much lower conductivity mantle and lithosphere. The dipole part of the field has the longest term changes, associated with geomagnetic excursions and reversals which require the axial dipole part of the field to vanish as it changes sign. Finite electrical conductivity of the mantle effectively filters variations in the core field on timescales much less than a year (Backus 1983). Thus, the internal part of the spectrum is greatly diminished in the frequency range dominated by the solar cycle, and magnetospheric processes. Above the insulating atmosphere is the relatively electrically conductive ionosphere, which supports Sq currents as a result of dayside solar heating. Outside the solid Earth, the magnetosphere, the manifestation of the core dynamo, is deformed and modulated by the solar wind, compressed on the Sun side, and elongated on the nightside. The volume within the magnetosphere contains the Van Allen radiation belts, which are layers of energetic charged particles: Usually, there are two main belts typically ranging in altitude from about 1000 to 60,000 km. In the outer belt, at a distance of about 3 Earth radii, the magnetospheric ring current which acts to oppose the main field is also modulated by solar activity. Magnetic fields generated in the magnetosphere and ionosphere propagate by induction into the conductive Earth, providing information on electrical conductivity variations in the crust and mantle. Satellites in Low Earth Orbit (LEO) observe magnetic fields above the ionosphere, but below the magnetospheric induction sources.

The various categories of external field signals are described in Table 1 and are further discussed in later sections. Note that even the largest external contributions are small in

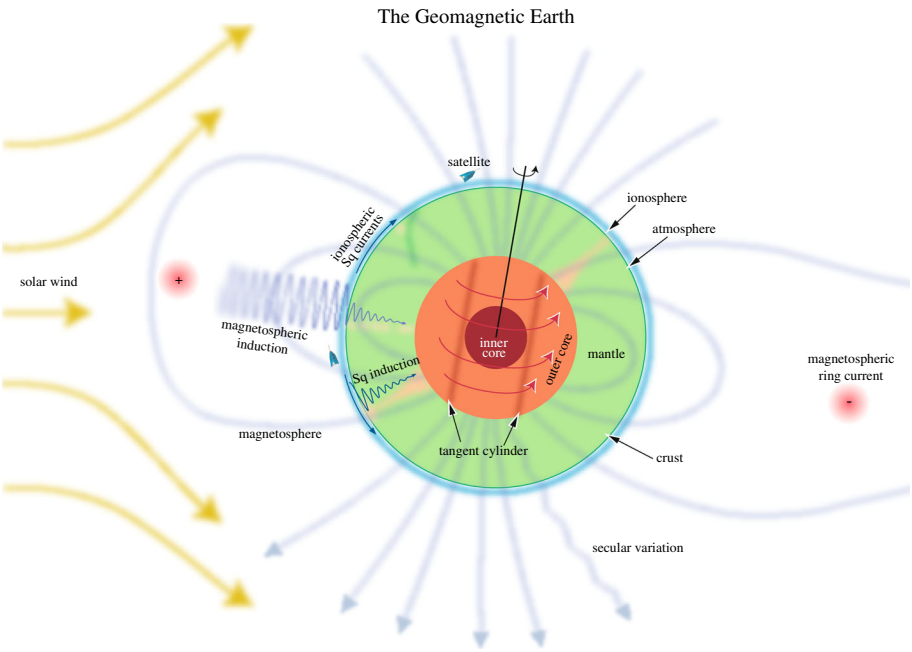

Fig. 2 Schematic view of geomagnetic sources (Constable and Constable 2004). The ring current and solar wind are not drawn to scale

Table 1 Typical properties of various external geomagnetic variations modified from Olsen (2007)

Type of variation	Symbol	Period or frequency	Amplitude	Skin depth
Solar cycle		11 years	10–20 nT	>2000 km
Annual		12 months	5 nT	1500–2000 km
Semiannual		6 months	5 nT	
Storm time	Dst	Hours to weeks	50–500 nT	300–1000 km
Regular daily		12 months	5 nT	
At mid-latitudes	Sq	24 h and harmonics	20–50 nT	300–600 km
At low latitudes	EEJ	12 months	50–100 nT	
Substorms	DP	10 min to 2 h	100 nT (1000 nT at p.l.)	100–300 km
Pulsations	ULF	0.3–600 s		20–100 km
Regular	pc	150–600 s (pc5)	10 nT (100 nT at p.l.)	
Continuous		45–150 s (pc4)	2 nT	
Pulsations		5–45 s (pc2,3)	0.5 nT	
		0.2–5 s (pc1)	0.1 nT	
Irregular pulsations	pi	1–150 s	1 nT	
Ionospheric Alfvén resonances	IAR	0.5–10 Hz		
Extreme low frequency	ELF Sferics	3 Hz–3 kHz	<0.1 nT	10 m to km
Schumann resonances		8 Hz and harmonics	<0.1 nT	
Plasmaspheric hiss		200 Hz–2 kHz		
Chorus, whistlers, lightning	VLF	3–30 kHz		m to 10s of m

Signals with significant latitude dependence are also given values at polar latitudes (p.l., $> 65°$)

comparison with the strength of the internal part, which currently ranges from about 22 μT over Brazil to more than 65 μT near the poles. Electromagnetic induction studies make use of external field variations with frequencies ranging from the solar cycle which has been used for geomagnetic depth sounding (GDS) through the 10^{-4}–10^{4} Hz frequency band widely used for magnetotelluric (MT) and audio-magnetotelluric (AMT) studies. At frequencies >1 Hz, the spectrum is dominated by sferics and anthropogenic noise. Locally, lightning energy peaks at about 10 kHz but rapid attenuation with distance in the Earth/ionosphere waveguide at this frequency impedes long-range detection (Shvets and Hayakawa 2011). By the time one reaches frequencies higher than 10^{4} Hz, the global EM spectrum becomes blue, rising in response to man-made signals. This dominance obscures any contributions from whistlers and dawn chorus, whose interactions with the dipole field and radiation belt particles are nonetheless important. In the spectrum of Fig. 1, one can clearly see a frequency separation in the various natural sources, with signal from magnetic storms, and daily variation in the ionosphere dying away around 1 Hz, and the sferics losing energy around 1–3 kHz. These are well known as "dead bands" with very low signal in the MT source field.

3 The Magnetosphere

As already noted, the magnetosphere is the region dominated by Earth's magnetic field. It sits in the solar wind which is the atmosphere of the Sun, a fully ionized, hot, collisionless, magnetized plasma. About 95 % of the plasma consists of protons and electrons in nearly equal numbers, and the remainder is mostly ionized helium with smaller numbers of heavier ions. The solar wind is supersonic above a few solar radii and is capable of carrying a large amount of kinetic and electrical energy. At Earth's orbit, the typical proton and electron densities are around 7 cm^{-3}, velocity about 440 km s^{-1}, producing a dynamic pressure of about 2 nPa. The interplanetary magnetic field (IMF) embedded in the plasma is around 7 nT (Hundhausen 1995). In Fig. 2, a charged particle approaching Earth from the sunward side will be deflected around Earth, but this simplistic view is missing key aspects of the dynamical process that shape the magnetosphere, including mechanisms for particles to populate the Van Allen radiation belts and associated magnetospheric ring current.

An accessible review of large-scale magnetospheric structure and dynamics (Russell 1995; Siscoe 2011) begins with the Chapman-Ferraro (CF) problem, ignoring the interplanetary magnetic field (IMF), treating the solar wind as electrically neutral (but ionized) and the magnetosphere as a vacuum. The dominant effect is then compression of field lines by the solar wind from the pressure of streams of particles which are repelled by the geomagnetic field at the magnetopause, generating the CF currents, and producing the magnetospheric cavity. The balance of internal magnetic pressure against that of the solar wind determines the size and shape of the CF magnetosphere boundary. The compression of the magnetic field on the sunward side is communicated across the vacuum to Earth via gradients in the magnetic field.

This CF base model does not include any effects of magnetic tension, and it must be modified to accommodate the fact that the high electrical conductivity and supersonic speeds in the solar wind cause the magnetic flux associated with the IMF to be carried along with the charged particles. The magnetosphere is not a closed system, the IMF drives the process known as magnetic reconnection, and this results in a partially open magnetosphere. Plasma particles can move freely along magnetic field lines, and the solar wind

energy flowing past Earth finds its way into the ionosphere and upper atmosphere. A view of the process is shown in animation of a 3D Unstructured-mesh Magnetosphere Simulation at http://svs.gsfc.nasa.gov/cgi-bin/details.cgi?aid=20057 (courtesy NASA/Goddard Space Flight Center Conceptual Image Lab) illustrating coronal mass ejection and the subsequent interaction of the solar wind with Earth's magnetic field. Fast material ejected from the Sun generates magnetic reconnection events between the IMF and the Earth's magnetic field, which eventually sends high-speed electrons and protons into the Earth's upper atmosphere to form aurora. The details are complex and depend on the orientation of the IMF, a feature which is absent from the simplified diagram shown in Fig. 2. A more detailed view of the magnetosphere is given in Fig. 3, and the basic magnetohydrodynamic (MHD) equations used to describe the magnetospheric and ionospheric plasmas are given in Chapter 1 of Kelley (2009). The numerous transport processes in this figure are complex and can produce drastic variations in the intensity of the radiation belts, especially the outer one, on timescales of minutes to decades. Daglis et al. (2007) provide a review of the key features of magnetic storms which generate some of the largest changes in magnetospheric fields.

The magnetotail seen on the nightside of Earth's magnetosphere results from the stretching of the planet's magnetic field by the solar wind. Two lobes with the magnetic field directed mainly sunward (the northern lobe) and anti-sunward (the southern lobe) contain low concentrations of cold particles, but are separated by a hot plasma sheet (mainly of solar origin) and containing a boundary layer current. Burst-like reconfiguration in the plasma sheet magnetic field arises from variations in the solar wind and

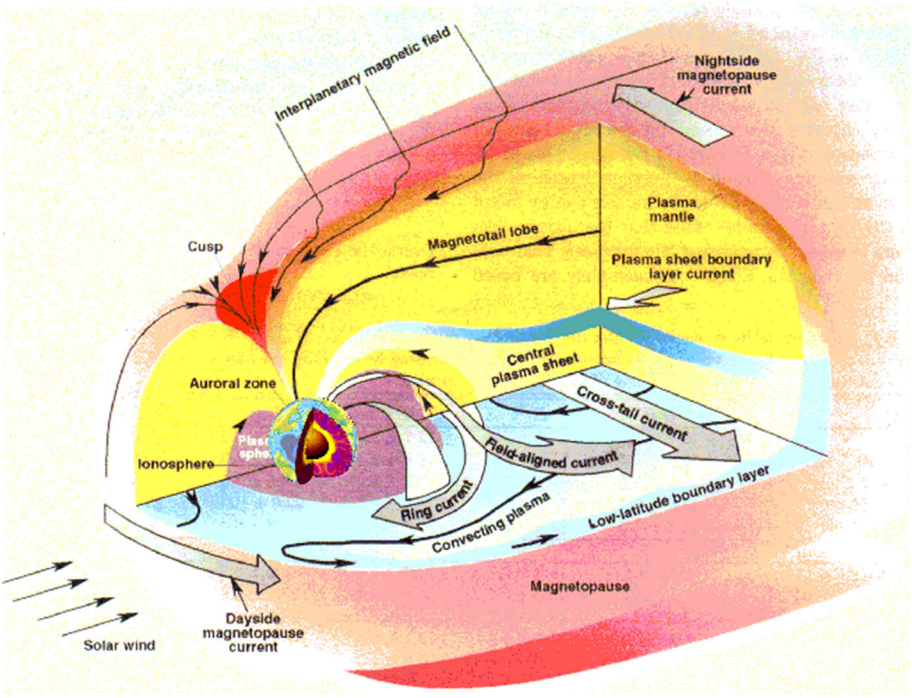

Fig. 3 Current systems in the magnetosphere after Fischbach et al. (1994)

interplanetary magnetic field, causing rapid plasma energization and acceleration. A portion of this energized charged particle population can propagate along magnetic field lines and bombard the planet's ionosphere and upper atmosphere to produce aurora in the polar cap region. Other energized particles invade the dipole-dominant inner magnetosphere, become trapped in the dipole magnetic field, and generate the ring current and radiation belts in the Earth's magnetosphere.

The broad spectral content of magnetospheric variations is apparent in Table 1. The solar cycle and solar rotation together with seasonal variations determine the composition of the solar wind and direction of the IMF. Magnetic storms energize the magnetosphere, and by extension the ionosphere at frequencies extending up through the ULF band. Geomagnetic micropulsations (McPherron 2005) Pc and Pi, which are, respectively, continuous or irregular, range from fractions of a second to minutes in period and fall in the ultralow frequency (ULF) band bordering on the extremely low frequencies (ELF, 3 Hz–3 kHz) of interest here. The pulsations are generated by characteristic resonant modes in the magnetospheric cavity. These modes couple to the ionosphere via field line resonances driving current in the ionosphere and are reradiated as electromagnetic energy observed at Earth's surface. The ULF and lower frequency variability set the background for ionospheric activity and coupling with the neutral atmosphere.

Space weather events are monitored by several global activity indices including the F10.7 solar flux at 2800 MHz (measured at Dominion Radio Astrophysical Observatory), the geomagnetic global Ap index (http://www.ngdc.noaa.gov/stp/GEOMAG/kp_ap.html), and the Dst index (http://wdc.kugi.kyoto-u.ac.jp/dstdir/). Space weather is also monitored by satellites, including the Advanced Composition Explorer (ACE) launched in 1997 and located at the L1 libration point (1.5×10^6 km distant where Earth and solar gravity fields are balanced). ACE will be superseded by the Deep Space Climate Observatory (DSCOVR) launched in February 2015 (Knipp and Biesecker 2015). Instrumentation on board includes a Faraday cup to monitor the speed and direction of positively charged solar wind particles, an electron spectrometer to monitor electrons, and a magnetometer to measure magnetic fields (http://www.nesdis.noaa.gov/DSCOVR/).

The Van Allen radiation belts are regions of trapped high-energy particles within the magnetosphere concentrated within two roughly toroidal shells extending to about 60° in geomagnetic latitude and separated in altitude by a so-called slot region containing little radiation. The particle locations are organized by the structure of Earth's magnetic field. Charged particles can move freely parallel to **B**, as magnetic field lines act like perfect conductors, transmitting perpendicular **E** fields and voltages across great distance, with no change in voltage along the field line. The presence of converging magnetic field lines near the poles slows particle motions and accelerates them back toward the equator. This process also causes particles to drift in longitude because the gyroradius is larger in weak fields, generating the ring current. The peak particle concentration and drift occurs near the equatorial plane, and its location is often expressed in terms of the L-parameter, which gives the distance in units of Earth radii from Earth's center where geomagnetic field lines cross the magnetic equator. The outer belt consists mainly of high-energy (0.1–10 MeV) electrons and peaks at L-parameters (McIlwain 1961) ranging from $\sim$3–6 (peaking at 4.5). Separating the inner and outer belts centered at $L = 2.2$ is a region with a minimum in electron flux with energies above 1 MeV. Particle density in the inner belt exhibits more high-energy protons and peaks at $L \sim 1.5$–2. There is no slot region for the ion density. The inner belt is considerably more stable than the outer one which can change radically over timescales of minutes to decades.

Much of our knowledge about the magnetosphere has been acquired during targeted satellite missions such as NASA's THEMIS and Van Allen Probes and ESA's Cluster which provide multipoint measurements within the radiation belts. For example, in 2013, the Van Allen Probes (a NASA mission initially named the Radiation Belt Storm Probes, RBSP) detected a transient third radiation belt, illustrating the dynamic nature of the belts. Electrons are energized either by radial diffusion or by local wave interactions with the latter mechanism observed on RBSP (Reeves et al. 2013). Under extreme space weather, the region can be temporarily filled with particles. Particles will gradually dissipate in the slot region as VLF waves interact with the electron gyromotion causing precipitation into the atmosphere where they are lost through collisions. The process by which electrons are lost from the radiation belt includes resonant interactions with plasmaspheric hiss, whistler mode chorus, and electromagnetic ion-cyclotron waves (Millan and Thorne 2007).

4 The Ionosphere

The ionosphere lies above the neutral atmosphere starting at about 50km elevation and forms the lowermost structure of the magnetosphere. The ionization which supplies its name is caused by solar radiation at ultraviolet, X-ray, and shorter wavelengths on the daylight side of Earth, which dislodges electrons from atmospheric atoms and molecules. The ionosphere is studied using both passive and active methods to monitor optical and radio emissions and response to probing via man-made radio sources at a range of frequencies.

Numerous observations have been used to build a basic empirical model of the ionosphere as a function of location, altitude, day of year, phase of sunspot cycle, and geomagnetic activity. COSPAR and URSI collaboratively sponsor the International Reference Ionosphere (IRI, http://ccmc.gsfc.nasa.gov/modelweb/ionos/iri.html) model, which is parameterized in terms of electron density, electron and ion temperatures, and ionic composition. Data contributing to this model provide a statistical description based on large number of observations coming from ground-based ionospheric sounding (ionosondes and numerous other data and products related to the ionosphere are archived at World Data Centers, see, e.g., http://www.ngdc.noaa.gov/stp/IONO/ionogram.html), by incoherent scatter radar at frequencies of 1–40 MHz from distributed ground arrays (e.g., EISCAT, Jicamarca, Arecibo, Millstone Hill, Malvern, St Santin), and by the coherent scatter Super Dual Auroral Radar Network (SuperDARN).

Sounding from the top side of the ionosphere has been possible since the launch of the first Alouette satellite mission in 1962. Numerous subsequent missions including Alouette 2, ISIS, and the 1972–1975 AEROS and AEROS B NASA satellites have been able to study the F region from above.

Figure 4 shows temperature and electron count with altitude from Earth surface to 600km elevation. The chemistry is variable with altitude (see, e.g., Torr 1979), but major impacts on the electromagnetic environment can be adequately understood in terms of the electron count and collisions between neutral and charged particles. A balance between new ionization and recombination processes determines the overall amount of ionization present (and thus the electrical conductivity), with the net number of positive and negative charges approximately balanced. Also in the ionosphere neutral gas density generally exceeds that of plasma, so the EM forces in plasma are minimal, and the role of neutral winds is important. Ionospheric plasma is more or less tied to Earth rotation because the magnetic field lines are frozen into the plasma.

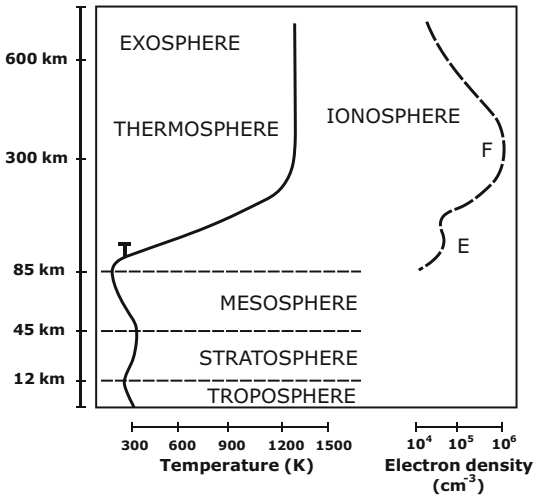

Fig. 4 Temperature and electron count as function of height in the ionosphere (from http://en.wikipedia.org/wiki/Ionosphere)

The structures in Fig. 4 are sensitive to geographic location, diurnal and seasonal effects in addition to the stage of sunspot cycle, the appearance of any solar flares, and their effect on solar wind. The electron count shows a minor peak in the E region and strong maximum in the F region, but again this is a simplified view. At night, the F layer is most important, and the amount of ionization in the D and E layers is low. Diurnal variations in ionospheric structure are outlined in Fig. 5, which shows how during the day the D and E layers are more heavily ionized, and the F layer is split into the F1 and F2 regions. The F2 layer is always present and is responsible for the refraction of radio waves. The D layer sits between about 60 and 90 km elevation and has low net ionization, but is subject to the most energetic radiations. During the daytime, the electron count in the D layer is greatly increased by solar radiation. The well-known diminished propagation of AM radio during the daytime compared with night arises from attenuation of short-wavelength radio signals through interactions with electrons. The AC electric field alternately accelerates and decelerates the electron for half a cycle, but if a collision between the electron and a neutral particle occurs during this process, the electron can be heated and the wave energy is dissipated. Solar proton events from solar flares can also cause high ionization in D layer at high and polar latitudes, which is bad for radio signal transmissions. During geomagnetic

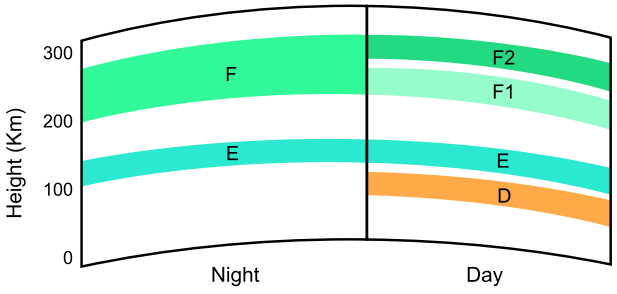

Fig. 5 Layer differences between night and daytime ionospheric structure (from http://en.wikipedia.org/wiki/Ionosphere)

storms, the F_2 layer becomes unstable and may disappear, and aurorae will be visible as already seen in the animation of coronal mass ejection.

Details of the ionospheric conductivity structure are strongly influenced by physical processes that depend on local time, latitude, season, and solar cycle. The conductivity is anisotropic because electron motions are bound to geomagnetic field lines, while the motion of positive ions is connected to the motion of the neutral gas. Conduction parallel to electric fields is known as the Pedersen conductivity and will be associated with Ohmic losses. In contrast, the Hall conductivity is perpendicular to **E** and the background magnetic field. Peak values of 10^{-3} S/m occur at 120–140 km altitude in sunlight, yielding an integrated conductance of about 50 S, but this is diminished by a factor of 10 or more on the nightside. Latitudinal variations are associated with the major Sq, auroral, and equatorial current systems, driven by seasonally varying atmospheric solar and lunar tides. Differential solar heating and lunar gravitational forcing move the ionospheric plasma against the main geomagnetic field modulating the conductivity, producing currents, and driving the dynamo process in the ionosphere.

Ionospheric structures are also perturbed by lightning. Return lightning strikes can enhance the E layer via direct heating arising from large motions of charge. VLF radio waves resulting from lightning are launched into the magnetosphere causing whistlers (Helliwell 2006). These are audio frequency dispersive waves which can interact with radiation belt particles causing them to precipitate into the ionosphere and perturb the D region via lightning-induced electron precipitation events (LEPs). Whistlers are now understood to play a key role in the dynamic interactions between hot and cold plasma in the magnetosphere contributing to losses and slot region development in the radiation belts.

5 The Global Electric Circuit

Historical developments in atmospheric electricity are described by Aplin et al. (2008), Williams (2010), and Williams (2009) and led to formalization of the idea of a global electric circuit (GEC) in the early twentieth century. It was already known at that time that a positive vertical potential gradient was present, ionization occurred in the air, and air had a finite electrical conductivity. Both the ground and ionosphere are relatively good electrical conductors, and the key controlling parameter for the GEC is the electrical conductivity of the atmosphere which is determined by the number of ions and their mobility and typically ranges from $\sim 10^{-15}$ S/m just above the ground to the comparatively highly conducting ionosphere ($\sim 10^{-7}$ S/m). The most important power source for the circuit is thunderstorm activity in tropospheric weather systems. Commonly visible cloud to ground, intracloud, and cloud-to-cloud lightning activity may encounter a resistance of several gigaohms in cloudy air (Bering et al. 1998). In contrast quasi-DC transient upward currents, from say 10 km altitude to the ionosphere, encounter a resistance of around 40 MΩ and continually generate upper atmospheric lightning connecting to the ionosphere. These return to the ground via the fair weather currents, across a global resistance of about 200 Ω away from the storms, as was proposed by C.T.R. Wilson in the 1920s. The circuit is completed by point discharge currents from ground to cloud.

Wilson's hypothesis was confirmed by the Carnegie curve, which correlated variations in the fair weather electric field over the open ocean with Universal Time fluctuations in thunderstorm activity peaking around 18:00 UT (Aplin et al. 2008). The electrical relaxation time of about 5–40 min near Earth's surface indicates the need for continued

excitation and the RC time constant of an equivalent electric circuit sets a timescale of order minutes for a quasi-static approximation of the system. For examples of such models, see Figure 2 in Aplin et al. (2008) or Figure 3 of Rycroft and Harrison (2012). The Wilson currents sustain an average electric potential at the ionosphere V_i of about 250 kV with respect to the ground, and the fair weather vertical return currents are ~ 2 pA/m^2.

The state of the magnetosphere and ionosphere described in the previous two sections provides the backdrop influencing the GEC which is illustrated by the cartoon in Fig. 6. Ionization in the atmosphere (and hence electric conductivity) is driven by the flux of galactic cosmic rays (GCRs) into the atmosphere, solar energetic protons, and nuclear decay gases from Earth's surface. Losses arise from recombination of positive and negative ions, and attachment to aerosol particles or droplets in clouds. Cosmic ray-produced ionization in the atmosphere is reviewed in Bazilevskaya et al. (2008). The ability for GCR particles to penetrate to the lower and middle atmospheres is controlled by their rigidity (the ratio of their momentum to charge), and the pitch angle of their momentum relative to the magnetic field in the access region; those with high rigidity can penetrate in equatorial regions, while much lower momentum is needed at higher geomagnetic latitudes. The flux of GCRs is controlled by time-varying structure of the heliosphere (and thus the IMF) and depends strongly on the solar cycle. At solar minima, the weaker field allows more GCRs to penetrate the heliosphere resulting in an increase of around 20 % at high latitude and around half that increase at mid to low latitudes. Thus, secondary DC effects in the global electric circuit are the dynamo interaction between the solar wind and the magnetosphere and dynamo interaction between atmospheric tides in the thermosphere (Bering et al. 1998). The latter are a product of gravitational and thermal forcing. Their amplitudes increase with altitude (as density correspondingly decreases) resulting in plasma motion across magnetic field lines. Atmospheric tides produce the seasonal variations and significant dependence of upper atmospheric ionospheric conductivity on geomagnetic latitude and local time.

Since the early twentieth century, measurement of cosmic ray (via ionization chambers) and related ion production (Bazilevskaya et al. 2008) have been conducted on balloons and

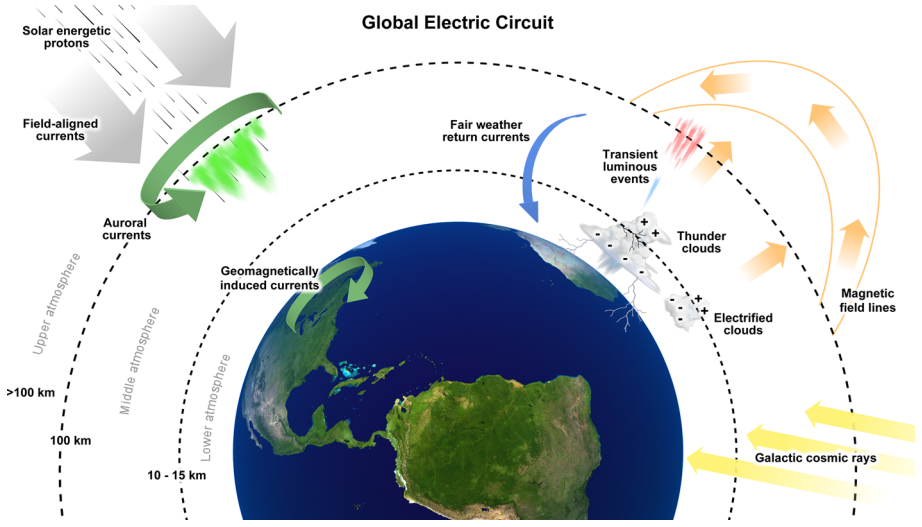

Fig. 6 The global electric circuit (credit: Jeffrey Forbes, University of Colorado at Boulder, http://sisko.colorado.edu/FESD/)

aircraft and on the ground. Combined with atmospheric electric field observations of potential difference between lowest and highest parts of their profiles, these provide information on temporal and spatial variability of electrical conductivity. When extrapolated to give V_i they indicate spatial variations of <20 % in amplitude at subauroral latitudes. Thunderstorm activity is correlated with seasonal temperature variations (Williams 1994) and peaks in the northern summer because it occurs preferentially over land. Corresponding seasonal differences are seen in the Carnegie curves. A recent paper by Baumgaertner et al. (2013) discusses an Earth system simulation model for atmospheric conductivity in the troposphere and stratosphere. The model incorporates representations of GCRs, solar proton events (Jackman et al. 2008), radon ionization, and loss from aerosols and including cloud effects as the next step in building a comprehensive DC global electric circuit model. Their modeling effort provides detailed geographic variability in atmospheric conductivity as well as a measure of anticipated temporal variations driven by seasonal aerosol and cloud variations. However, it does not include the effects of conductivity inside thunderstorms because of lack of definitive knowledge in this area.

The satellite and space shuttle era introduced an external vantage point initially stimulating optical studies of transient luminous events (TLEs) or upper atmosphere/ ionospheric lightning above thunderstorms. This led to the identification of sprites, blue jets, ELVES, and other such phenomena. Airborne and space-borne optical detectors and radio frequency (RF) measurements were launched to study them. These have limited spatial and temporal coverage, making complementary ELF ground-based observations an important tool for monitoring global thunderstorm activity. Location and timing of global lightning activity can be monitored using remote magnetic measurements. Mathematical descriptions of the propagation of signals from individual lightning strikes are readily formulated for a spherical ionospheric cavity, but for greater accuracy in locating the sources it is necessary to take account of rotation and day/night asymmetry in ionospheric structure.

5.1 Global Electromagnetic Resonances and Transient Luminous Events

Lightning generates a broad spectrum of electromagnetic radiation. The AC part of the GEC is dominated by sferics, radio waves in the upper atmosphere at frequencies below 10 kHz. The roughly spherical dielectric cavity bounded by the ground and the ionosphere acts as a waveguide for EM radiation produced by lightning, producing resonances at around 8 Hz and its harmonics as was predicted by W.O. Schumann in 1952. The frequency of the resonance is determined by the time for electromagnetic radiation to travel around the Earth. A transverse or vertical resonance also occurs at 1.7–2.0 kHz arising from reflections near the storm between the variable height lower boundary of the ionosphere and the ground and exhibiting line splitting due to 3D structure. Whistlers are also a product of lightning, but they are not confined to the atmosphere. They are EM waves with a continuous tone beginning at about 10 kHz and decreasing to a few hundred Hz over a few seconds. The term whistler arises from their detection as audio signals on phone lines. High-frequency sferics pass through the ionospheric layers rather than being reflected, evolving into a whistler from dispersive interactions within the plasmasphere.

Since the early 1960s, there have been numerous efforts in measuring the signals generated by sferics in vertical electric and horizontal magnetic fields. Early progress in both observational and theoretical work on the Schumann resonance was reviewed by Madden and Thompson (1965), at which time it was already known that the resonance and its harmonics had a Q factor of 4–5 that the resonant frequencies exhibited diurnal variations and theory was extended to allow for structural asymmetry in the ionosphere cavity.

Updated treatment of the theory and data processing is given in recent monographs (Nickolaenko and Hayakawa 2002, 2014), and Surkov and Hayakawa (2014) who provide thorough descriptions of more modern observations and data processing.

The GEC proposed by Wilson (1925) also predicted brief flashes of light above large thunderstorms, and with the advent of the space shuttle video imagery and optical detectors on satellites (Optical Transient Detector, 1995–2003, (Boccippio et al. 2000) and the Lightning Imaging Sensor from 1998–2003 on NASA's TRMM mission), we now know that these take astonishingly beautiful and diverse forms (Fig. 7). Sprites, elves, blue jets, and gigantic jets are transient luminous event (TLEs) caused by high-altitude breakdown associated with large thunderstorms and mesoscale convective systems (Boccippio et al. 1995; Williams 2001). The altitude of TLEs is limited by the presence of the conducting ionosphere, which reflects EM radiation. The discovery of sprites in 1989 (Franz et al. 1990) has led to significant new activity studying the GEC and numerous papers on this topic. Rodger (1999) summarizes the first observations and links made between optical sprite observations and excitations of transient Schumann resonance known as Q-bursts (Boccippio et al. 1995). Theoretical models of conditions leading to production of TLEs have evolved since their discovery and are discussed by Pasko (2010).

The link between excitation of Schumann resonance and TLEs has led to renewed efforts since the early 1990s to monitor such events via remote electromagnetic sensing of vertical electric and horizontal magnetic field components. Magnetic field measurements are generally taken using ground-based induction coil magnetometers which are best suited

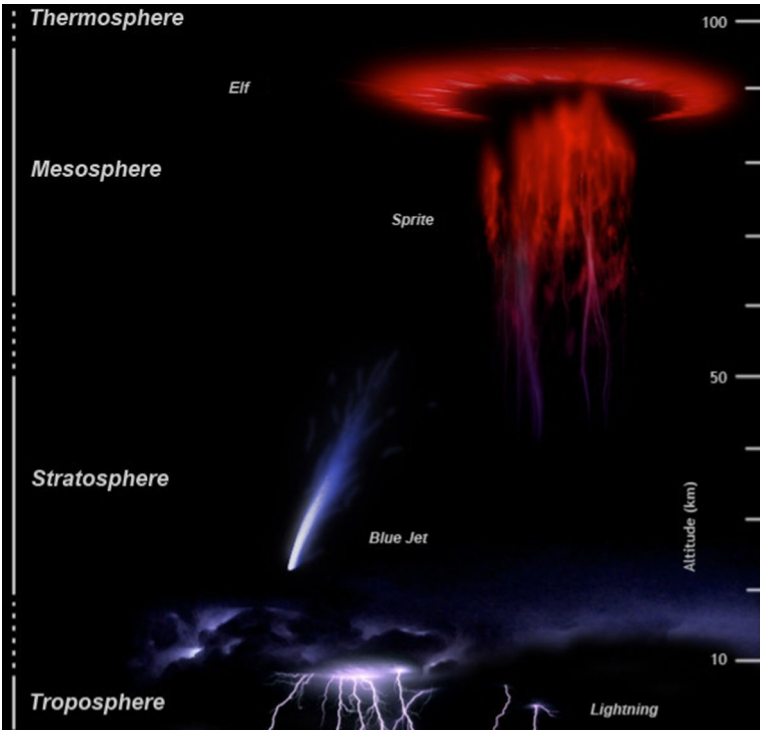

Fig. 7 TLEs in the upper atmosphere (from http://en.wikipedia.org/wiki/Upper-atmospheric_lightning)

for observations in this frequency range (Constable 2011; Ferguson 2012). Examples of simultaneous magnetic time series are given in Fig. 8, and such observations can be used to remotely detect monitor Q-bursts and build maps of global lightning occurrence, e.g., Füllekrug and Constable (2000), Williams et al. (2007), Whitley et al. (2011). Shvets and Hayakawa (2011) describe the formulation and application of the inverse problem to detect both location and moment of lightning under the assumption of a uniform ionospheric cavity using VLF and ELF band observations.

6 Summary of Relevance to Climate and Induction Studies

This review has emphasized the origin of electromagnetic signals of importance to induction studies at frequencies above 1 Hz, but setting them in the context of longer period ionospheric and magnetospheric variations that influence activity levels. The size of the EM signals in this frequency range is controlled by the strength of the global electric circuit and influenced by the numerous external processes which produce temporal variations on diurnal, seasonal, and solar cycles. In the northern hemisphere for the AMT frequency range (1–10 kHz), the signal amplitude is greater at night and during the summer months than during the daytime and winter.

As was noted in the Sect. 1, AMT induction studies make use of ELF and VLF source fields to study the near-surface conductivity structure on local, regional, and global scales. These rely on the plane wave approximation of a uniform source field (well satisfied by the global Schumann resonance signals). The electromagnetic skin depth z_s determines the decay of field amplitude with depth (specified here in m) in the Earth and depends on frequency and conductivity via

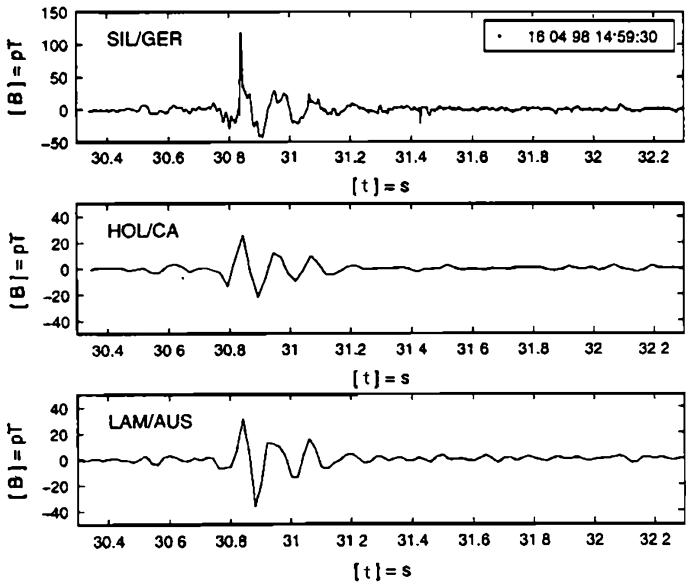

Fig. 8 Time series showing excitation of Schumann resonance in horizontal magnetic field observations from Germany, California, and Australia (from Fullekrug 2000)

$$z_s \approx 500\sqrt{1/\sigma f}. \quad (1)$$

Conductivity is sensitive to mineral composition, salinity, temperature, fluids, water, and melt, and suitable targets for study at frequencies above 1 Hz generally lie no deeper than a few km. This dictates the major emphasis on economic, environmental, and engineering applications and hazard assessments in the form of earthquake and volcano monitoring. Numerous case studies have been published, for example, of mineral exploration, direct imaging of ore bodies, petroleum exploration, geothermal and groundwater assessments. Some entry points to the vast literature on these topics can be found in Ferguson et al. (2012), Nabighian (1988), Nabighian (1991), McNeill and Labson (1991), Nobes (1996), and Pellerin (2002). A further limitation on induction studies is the size of the atmospheric source signal which falls off rapidly at around 1 kHz (the MT dead band), which has led to the development of robust processing techniques in attempts to extract reliable MT response estimates (García and Jones 2002, 2005, 2008). Other alternatives include making use of some stronger anthropogenically generated source fields via the Radio Magnetotelluric (RMT) method (Bastani and Pedersen 2001; Pedersen et al. 2006; Zacher et al. 1996), which makes use of civilian and military radio transmitters in the 10 kHz–1 MHz range. The plane wave approximation for the source is considered adequate, provided that the transmitter is at a distance $>7\,z_s$ (Tezkan and Saraev 2008) and RMT is useful for mapping very near-surface contamination which can pose environmental hazards.

Important applications of the global electric circuit remain in mapping the locations and power of global thunderstorm activity using electromagnetic methods and in the potential for detection of changes in the mesosphere associated with global climate change. Such activities still require consistent effort and the establishment of global networks to monitor and detect changes, for improved study of the GEC. Several complexities of ionosphere structure have yet to be incorporated in global lightning studies. In particular, the approximation by a uniform bounded ionospheric cavity fails to take into account diurnal variations in dimensions and structure. The detection of Schumann resonance signals by the C/NOFS satellite at over 400 km altitude (Simões et al. 2011) also draws attention to the diffuse boundary for the ionosphere and associated more gradual increase in electrical conductivity with altitude. Additional complexity not explicitly considered in the modeling is the effect of global variations in near-surface Earth conductivity, and this highlights the possibility for EM induction studies to play some role in climate studies. There is considerable scope for improving global surface conductance models over those in current use (Everett et al. 2003; Olsen and Kuvshinov 2004).

Acknowledgments I thank Ciaran Beggan, Steven Constable, Monika Korte, and Tom Nielsen for useful discussions, the Alexander von Humboldt Foundation for funding that supported this endeavor, and both administrative and research staff at GFZ, Potsdam for their hospitality, and collegial support. I would also like to acknowledge the unprecedented opportunity provided by the 2014 EM Induction workshop organizing committee to work on a review outside my usual area of expertise. I very much appreciated the useful comments on both clarity and content from two anonymous reviewers.

References

Aplin KL, Harrison RG, Rycroft MJ (2008) Investigating Earth's atmospheric electricity: a role model for planetary studies. Space Sci Rev 137(1–4):11–27

Backus G, Parker RL, Constable C (1996) Foundations of geomagnetism, digitally printed 1st pbk. edn. Cambridge University Press, Cambridge

Backus GE (1983) Application of mantle filter theory to the magnetic jerk of 1969. Geophys J Int 74(3):713–746
Bastani M, Pedersen LB (2001) Estimation of magnetotelluric transfer functions from radio transmitters. Geophysics 66(4):1038–1051
Baumgaertner AJG, Thayer JP, Neely RR, Lucas G (2013) Toward a comprehensive global electric circuit model: atmospheric conductivity and its variability in CESM1(WACCM) model simulations. J Geophys Res Atmos 118(16):9221–9232
Bazilevskaya GA, Usoskin IG, Flückiger EO, Harrison RG, Desorgher L, Bütikofer R, Krainev MB, Makhmutov VS, Stozhkov YI, Svirzhevskaya AK, Svirzhevsky NS, Kovaltsov GA (2008) Cosmic ray induced ion production in the atmosphere. Space Sci Rev 137(1–4):149–173
Bering EA III, Few AA, Benbrook JR (1998) The global electric circuit. Phys Today 51(10):24
Boccippio DJ, Williams ER, Heckman SJ, Lyons WA, Baker IT, Boldi R (1995) Sprites, ELF transients, and positive ground strokes. Science 269(5227):1088–1091
Boccippio DJ, Koshak W, Blakeslee R, Driscoll K, Mach D, Buechler D, Boeck W, Christian HJ, Goodman SJ (2000) The optical transient detector (OTD): instrument characteristics and cross-sensor validation. J Atmos Ocean Technol 17(4):441–458
Chapman S, Bartels J (1940) Geomagnetism, vol 1. Clarendon Press, Oxford
Chave AD, Jones AG (eds) (2012) The magnetotelluric method. Theory and practice. Cambridge University Press, Cambridge
Constable CG, Constable SC (2004) Satellite magnetic field measurements: applications in studying the deep earth. In: The state of the planet: frontiers and challenges in geophysics. American Geophysical Union, International Union of Geodesy and Geophysics, Washington, DC
Constable S (2007) Geomagnetism. In: Schubert G, Kono M (eds) Treatise on geophysics. Elsevier, Amsterdam, pp 237–276
Constable S (2011) EM instrumentation. In: Gupta HK (ed) Encyclopedia of solid earth geophysics. Springer, Dordrecht, pp 604–608
Constable SC, Parker RL, Constable CG (1987) Occam's inversion: a practical algorithm for generating smooth models from electromagnetic sounding data. Geophysics 52(3):289–300
Daglis IA, Tsurutani BT, Gonzalez WD, Kozyra JU, Orsini S, Cladis J, Kamide Y, Henderson MG, Vassiliadis D (2007) Key features of intense geospace storms–a comparative study of a solar maximum and a solar minimum storm. Planet Space Sci 55(1–2):32–52
Everett ME, Constable S, Constable CG (2003) Effects of near-surface conductance on global satellite induction responses. Geophys J Int 153(1):277–286
Ferguson IJ (2012) Instrumentation and field procedures. In: Chave AD, Jones AG (eds) The magnetotelluric method. Cambridge University Press, Cambridge, pp 421–473
Ferguson IJ, Jones AG, Chave AD (2012) Case histories and geological applications. In: Chave AD, Jones AG (eds) The magnetotelluric method. Cambridge University Press, Cambridge, pp 480–536
Fischbach E, Kloor H, Langel RA, Lui ATY, Peredo M (1994) New geomagnetic limits on the photon mass and on long-range forces coexisting with electromagnetism. Phys Rev Lett 73(4):514–517
Franz RC, Nemzek RJ, Winckler JR (1990) Television image of a large upward electrical discharge above a thunderstorm system. Science 249(4964):48–51
Füllekrug M, Constable S (2000) Global triangulation of intense lightning discharges. Geophys Res Lett 27(3):333–336
García X, Jones AG (2002) Atmospheric sources for audio-magnetotelluric (AMT) sounding. Geophysics 67(2):448–458
García X, Jones AG (2005) A new methodology for the acquisition and processing of audio-magnetotelluric (AMT) data in the AMT dead band. Geophysics 70(5):G119–G126
García X, Jones AG (2008) Robust processing of magnetotelluric data in the AMT dead band using the continuous wavelet transform. Geophysics 73(6):F223–F234
Gubbins D, Herrero-Bervera E (eds) (2007) Encyclopedia of geomagnetism and paleomagnetism. Springer, Berlin
Helliwell RA (2006) Whistlers and related ionospheric phenomena. Dover, Mineola
Hulot G, Balogh A, Christensen UR, Constable C, Mandea M, Olsen N (eds) (2010) Terrestrial magnetism. Space science series of ISSI. Springer, Berlin
Hundhausen AJ (1995) The solar wind. In: Kivelson MG, Russell CT (eds) Introduction to space physics. Cambridge University Press, Cambridge
Jackman CH, Marsh DR, Vitt FM, Garcia RR, Fleming EL, Labow GJ, Randall CE, López-Puertas M, Funke B, von Clarmann T, Stiller GP (2008) Short- and medium-term atmospheric constituent effects of very large solar proton events. Atmos Chem Phys 8(3):765–785
Jacobs JA (1987) Geomagnetism. Academic Press, New York

Kelley MC (2009) The Earth's ionosphere: plasma physics and electrodynamics, 2nd edn. Elsevier, Amsterdam
Kivelson MG, Russell CT (eds) (1995) Introduction to space physics. Cambridge University Press, Cambridge
Knipp DJ, Biesecker DA (2015) Changing of the guard: Satellite will warn Earth of solar storms. EOS 96
Kono M (ed) (2007) Geomagnetism, treatise on geophysics, vol 5, 1st edn. Elsevier, Amsterdam
Madden T, Thompson W (1965) Low-frequency electromagnetic oscillations of the Earth-ionosphere cavity. Rev Geophys 3(2):211
Matsushita S, Campbell WH (eds) (1967) Physics of geomagnetic phenomena, vol 94. Academic Press, New York
McIlwain CE (1961) Coordinates for mapping the distribution of magnetically trapped particles. J Geophys Res 66(11):3681–3691
McNeill JD, Labson VF (1991) Geological mapping using VLF radio fields. In: Nabighian MN (ed) Electromagnetic methods in applied geophysics. Society of Exploration Geophysicists, Tulsa
McPherron R (2005) Magnetic pulsations: their sources and relation to solar wind and geomagnetic activity. Surv Geophys 26(5):545–592
Millan RM, Thorne RM (2007) Review of radiation belt relativistic electron losses. J Atmos Solar Terr Phys 69(3):362–377
Nabighian MN (ed) (1988) Electromagnetic methods in applied geophysics. Voume 1, theory. Society of Exploration Geophysicists
Nabighian MN (ed) (1991) Electromagnetic methods in applied geophysics. Volume 2, Application, Parts A and B, Society of Exploration Geophysicists
Nickolaenko A, Hayakawa M (2014) Schumann resonance for Tyros. Springer, Tokyo
Nickolaenko AP, Hayakawa M (2002) Resonances in the Earth-ionosphere cavity. Kluwer, Dordrecht
Nobes DC (1996) Troubled waters: environmental applications of electrical and electromagnetic methods. Surv Geophys 17(4):393–454
Olsen N (2007) Natural sources for electromagnetic induction studies. In: Gubbins D, Herrero-Bervera E (eds) Encyclopedia of geomagnetism and paleomagnetism. Springer, pp 696–700 (563)
Olsen N, Kuvshinov A (2004) Modeling the ocean effect of geomagnetic storms. Earth Planets Space 56(5):525–530
Olsen N, Hulot G, Sabaka TJ (2010) Sources of the geomagnetic field and the modern data that enable their investigation. In: Freeden W, Nashed MZ, Sonar T (eds) Handbook of geomathematics. Springer, Berlin
Pasko VP (2010) Recent advances in theory of transient luminous events. J Geophys Res 115:A00E35
Pedersen L, Bastani M, Dynesius L (2006) Some characteristics of the electromagnetic field from radio transmitters in Europe. Geophysics 71(6):G279–G284
Pellerin L (2002) Applications of electrical and electromagnetic methods for environmental and geotechnical investigations. Surv Geophys 23(2–3):101–132
Pozzo M, Davies C, Gubbins D, Alfè D (2012) Thermal and electrical conductivity of iron at Earth's core conditions. Nature 485(7398):355–358
Reeves GD, Spence HE, Henderson MG, Morley SK, Friedel RHW, Funsten HO, Baker DN, Kanekal SG, Blake JB, Fennell JF, Claudepierre SG, Thorne RM, Turner DL, Kletzing CA, Kurth WS, Larsen BA, Niehof JT (2013) Electron acceleration in the heart of the van Allen radiation belts. Science 341(6149):991–994
Rodger CJ (1999) Red sprites, upward lightning, and VLF perturbations. Rev Geophys 37(3):317
Rodi W, Mackie RL (2001) Nonlinear conjugate gradients algorithm for 2-D magnetotelluric inversion. Geophysics 66(1):174–187
Rodi W, Mackie RL (2012) The inverse problem. In: Chave AD, Jones AG (eds) The magnetotelluric method. Cambridge University Press, Cambridge
Russell CT (1995) A brief history of solar-terrestrial physics. In: Kivelson MG, Russell CT (eds) Introduction to space physics. Cambridge University Press, Cambridge
Rycroft MJ, Harrison RG (2012) Electromagnetic atmosphere-plasma coupling: the global atmospheric electric circuit. Space Sci Rev 168(1–4):363–384
Sabaka TJ, Hulot G, Olsen N (2010) Mathematical properties relevant to geomagnetic field modeling. Handbook of geomathematics. Springer, Berlin, pp 503–538
Shvets A, Hayakawa M (2011) Global lightning activity on the basis of inversions of natural ELF electromagnetic data observed at multiple stations around the world. Surv Geophys 32(6):705–732
Simões F, Pfaff R, Freudenreich H (2011) Satellite observations of Schumann resonances in the Earth's ionosphere. Geophysical Res Lett 38. doi:10.1029/2011GL049668
Simpson F, Bahr K (2005) Practical magnetotellurics. Cambridge University Press, Cambridge

Siripunvaraporn W (2012) Three-dimensional magnetotelluric inversion: an introductory guide for developers and users. Surv Geophys 33(1):5–27
Siscoe G (2011) Aspects of global coherence of magnetospheric behavior. J Atmos Solar Terr Phys 73(4):402–419
Surkov V, Hayakawa M (2014) Ultra and extremely low frequency electromagnetic fields. Springer, Berlin
Tezkan B, Saraev A (2008) A new broadband radiomagnetotelluric instrument: applications to near surface investigations. Near Surface Geophys
Torr DG (1979) Ionospheric chemistry. Rev Geophys 17(4):510–521
Vozoff K (1991) The magnetotelluric method. In: Nabighian MN (ed) Electromagnetic methods in applied geophysics. Society of Exploration Geophysicists, Tulsa, pp 641–711
Weidelt P, Chave AD (2012) The magnetotelluric response function. In: Chave AD, Jones AG (eds) The magnetotelluric method. Cambridge University Press, Cambridge
Whitley T, Füllekrug M, Rycroft M, Bennett A, Wyatt F, Elliott D, Heinson G, Hitchman A, Lewis A, Sefako R, Fourie P, Dyers J, Thomson A, Flower S (2011) Worldwide extremely low frequency magnetic field sensor network for sprite studies. Radio Sci 46. doi:10.1029/2010RS004523
Williams ER (1994) Global circuit response to seasonal variations in global surface air temperature. Mon Weather Rev 122(8):1917–1929
Williams ER (2001) Sprites, elves and glow discharge tubes. Phys Today
Williams ER (2009) CTR Wilson versus GC Simpson: fifty years of controversy in atmospheric electricity. Atmos Res 91(2–4):259–271
Williams ER (2010) Origin and context of C. T. R. Wilson's ideas on electron runaway in thunderclouds. J Geophys Res Space Phys 115. doi:10.1029/2009JA014581
Williams ER, Mushtak VC, Boldi R, Dowden RL, Kawasaki ZI (2007) Sprite lightning heard round the world by Schumann resonance methods. Radio Sci 42. doi:10.1029/2006RS003498
Zacher G, Tezkan B, Neubauer FM, Hordt A, Müller I (1996) Radiomagnetotellurics, a powerful tool for waste site exploration. Eur J Environ Eng Geophys 1(2):139–160